Relationships between Low-Frequency Variability in the Southern Hemisphere and Sea Surface Temperature Anomalies

KINGTSE C. MO

Climate Prediction Center, NCEP/NWS/NOAA, Camp Springs, Maryland

(Manuscript received 9 September 1999, in final form 24 January 2000)

ABSTRACT

Long-term trends and interannual variations of circulation anomalies in the Southern Hemisphere are examined using the National Centers for Environmental Prediction–National Center for Atmospheric Research reanalysis from 1949 to 1998. The changes in planetary circulation regimes are linked to global sea surface temperature anomalies (SSTAs).

Empirical orthogonal function (EOF) analysis was performed on 500-hPa height anomalies. The leading mode EOF1 shows a strong zonal symmetry with a phase reversal between height anomalies in high and midlatitudes. Apart from zonal symmetry, a zonal wavenumber 3 is evident with three centers located in three southern oceans. In the low-frequency band with fluctuations longer than 60 months, EOF1 is associated with the second rotated EOF mode of SSTAs with positive loadings over three southern oceans and negative loadings in the North Pacific and the North Atlantic.

The next two modes are the Pacific–South American (PSA) patterns. They depict wave-3 patterns in quadrature with each other and a well-defined wave train from the tropical Pacific to Argentina with large amplitudes in the Pacific–South American sector. On decadal timescales, the abrupt warming over the central and eastern Pacific is related to the strengthening of PSA1. In the interannual band, PSA1 is associated with the low-frequency part of El Niño–Southern Oscillation (ENSO) variability with the dominant period of 40–48 months. PSA2 is associated with the quasi-biennial component of ENSO variability with a period of 26 months.

1. Introduction

Van Loon et al. (1993) examined climate variations of atmospheric circulation over the Southern Hemisphere (SH) in the Australian dataset from 1972 to 1989. They discovered a sudden change in the SH circulation anomalies after 1976. The zonal wave 3 intensified in the SH midlatitudes, while the sea level pressure fell over Antarctica. By comparison with station data, they concluded that these changes were real and not a result of the Australian analysis. Hurrell and van Loon (1994) later extended the above study to include changes in the semiannual cycle.

Recently, Karoly et al. (1996) used monthly mean surface pressure reports from station observations in the SH to study circulation changes on decadal timescales. The leading mode responsible for interannual and interdecadal variations of the SH circulation is related to El Niño–Southern Oscillation (ENSO). The second mode shows a downward trend of sea level pressure anomalies in the SH high latitudes since 1976.

Corresponding author address: Kingtse Mo, Climate Prediction Center, NCEP/NWS/NOAA, 5200 Auth Rd., Camp Springs, MD 20746.
E-mail: kmo@ncep.noaa.gov

Are these changes related to the decadal and interannual changes in global sea surface temperature anomalies (SSTAs)? Zhang et al. (1997) described the leading SSTA mode in the low-frequency band for fluctuations longer than 6 yr. It shows warming in the eastern Pacific and cooling in the North Pacific from 1976 to the present. This mode is different from interannual variability in the high-frequency band (less than 6 yr). In that band, the leading mode is related to ENSO.

In the Northern Hemisphere, many studies have linked circulation changes to SSTA (Zhang et al. 1997; Trenberth and Hurrell 1994). Jones and Allan (1998) did a comprehensive review of long-term climate variability in the SH. Allan et al. (1995) and Reason et al. (1996) examined interdecadal changes in the Indian Ocean and found opposite phases of anomalies between the early period 1921–41 and the recent period 1963–83. Garreaud and Battisti (1999) extended the study of Zhang et al. (1997) to examine anomalies in the SH. In the high-frequency band, which consists of fluctuations shorter than 6 yr, the dominant mode is a wave train extending from the Pacific to South America. This wave train has been identified as the Pacific–South American pattern (PSA), which is the typical response to ENSO (Karoly 1989). The low-frequency mode is described as an ENSO-like pattern related to wave–mean flow in-

teractions in high latitudes. Their patterns are keyed to the SSTA cold tongue index in the eastern Pacific. SSTAs elsewhere are taken into account implicitly through the residual term.

Recently, the National Centers for Environmental Prediction–National Center for Atmospheric Research (NCEP–NCAR) reanalysis (Kalnay et al. 1996) from 1949 to 1998 has been completed. The reanalysis was performed using a fixed model and a fixed assimilation scheme. However, the reanalysis products can still be affected by changes in the observational input data. If the circulation changes are linked to the boundary forcing such as SSTAs, then these changes are more likely to be real and physically meaningful.

This paper examines long-term trends and interannual variations of large-scale circulation regimes in the Southern Hemisphere from 1949 to the present using the NCEP–NCAR reanalysis. The changes in circulation regimes are linked to changes in SSTAs. In the low-frequency band, there are two SSTA modes related to the long-term trends observed in the SH circulation. One mode is associated with gradual SST warming in three southern oceans and the other mode displays the abrupt warming in the central and eastern Pacific after 1976. The changes in the interannual band are linked to a low-frequency mode with a period of 48 months and the quasi-biennial component of ENSO variability (Rasmusson et al. 1990). Results here are compared to findings of Garreaud and Battisti (1999).

2. Data and procedures

The data used to examine circulation features are monthly mean heights, winds and sea level pressure from the NCEP–NCAR reanalysis for the period 1949 to 1998 (Kalnay et al. 1996). The horizontal resolution is 2.5° latitude by 2.5° longitude. There is an error in the reanalysis assimilation from 1979 to 1992. The Australian surface pressure bogus data over the southern oceans were read in 180° out of phase. While this error will impact daily analyses, it has minimal impact on monthly mean fields or low-frequency variability. Sea surface temperature data were obtained from the historical reconstruction based on empirical orthogonal functions (EOFs) by Smith et al. (1996). The SST data are on a 2° latitude by 2° longitude grid and are available from 1950 to the present. The annual cycle was removed from the monthly mean datasets by subtracting climatological monthly means from individual months. To obtain the interannual signal, data were filtered using the minimum bias window developed by Papoulis (1973) to retain periods less than 60 months. This band is referred to as the high-frequency band. The low-pass filtered signals were obtained as the departures from the high-pass filtered data. This band is referred to as the low-frequency band.

EOF analysis was performed on the seasonal mean 500-hPa height anomalies for the SH (90°S–equator) and SSTAs for the domain (40°S–60°N). All seasons were pooled together. To reduce the matrix size, the horizontal resolution was reduced to $5° \times 5°$ for height anomalies and $4° \times 4°$ for SSTAs. Anomalies were not normalized but a latitudinal cosine weighting factor was used in computing the covariance matrix. Varimax rotation was performed on eigenvectors. The number of modes selected for rotation was determined by the criterion established by O'Lenic and Livezey (1988).

To determine modes associated with ENSO variability, singular spectrum analysis (SSA) was used. SSA was also used by Rasmusson et al. (1990) to determine oscillatory modes related to ENSO variability. SSA is basically a statistical technique related to EOF analysis to determine oscillatory modes in the time space (Vautard and Ghil 1989; Vautard et al. 1992). Quasiperiodic signals appear as pairs of degenerate eigenmodes and their corresponding eigenfunctions in the time domain (T-EOFs) are in quadrature with each other. The original time series can be projected onto T-EOFs to obtain principal components in the time domain (T-PCs). For details, readers are referred to Vautard and Ghil (1989). A window length of 61 months was used. Results are not sensitive to the particular window length used.

3. Circulation regimes in the Southern Hemisphere

As noted by Lau et al. (1994), the seasonal variation of EOFs is not large in the SH. The first 3 EOFs (Figs. 1a–c) are the same for all seasons together or for the SH winter (June–August). They explain 20%, 13%, and 11% of the total variance respectively. Varimax rotation was performed using 10 EOFs. All three EOFs appear also as rotated EOFs but they appear in different sequence. The first EOF is the fourth rotated EOF (REOF) and the second EOF is the first REOF. EOF3 appears as REOF5. To test the robustness of the results, EOF analysis was also performed on the seasonal mean 500-hPa height anomalies for the European Centre for Medium-Range Weather Forecasting (ECMWF) reanalysis from 1979 to 1993. The ECMWF analysis used a different assimilation system and input data from the NCEP. The first three EOFs are given in Figs. 1d–f. They explain 27%, 12.7%, and 10% of the total variance. There are differences, but major features are similar and can be found in EOFs from both reanalyses. These EOFs resemble the EOFs obtained by Kidson (1988a, 1999), Kiladis and Mo (1998), and Rogers and van Loon (1982), though different datasets and data periods were used.

EOF1 (Figs. 1a and 1d) shows a strong zonal symmetry with a phase reversal between high and midlatitudes. Apart from zonal symmetry, a zonal wave 3 is evident with three centers of action located in three southern oceans. EOF1 is the leading mode in the low-frequency band (Kiladis and Mo 1998). It resembles REOF2 obtained by Karoly et al. (1996) using the sta-

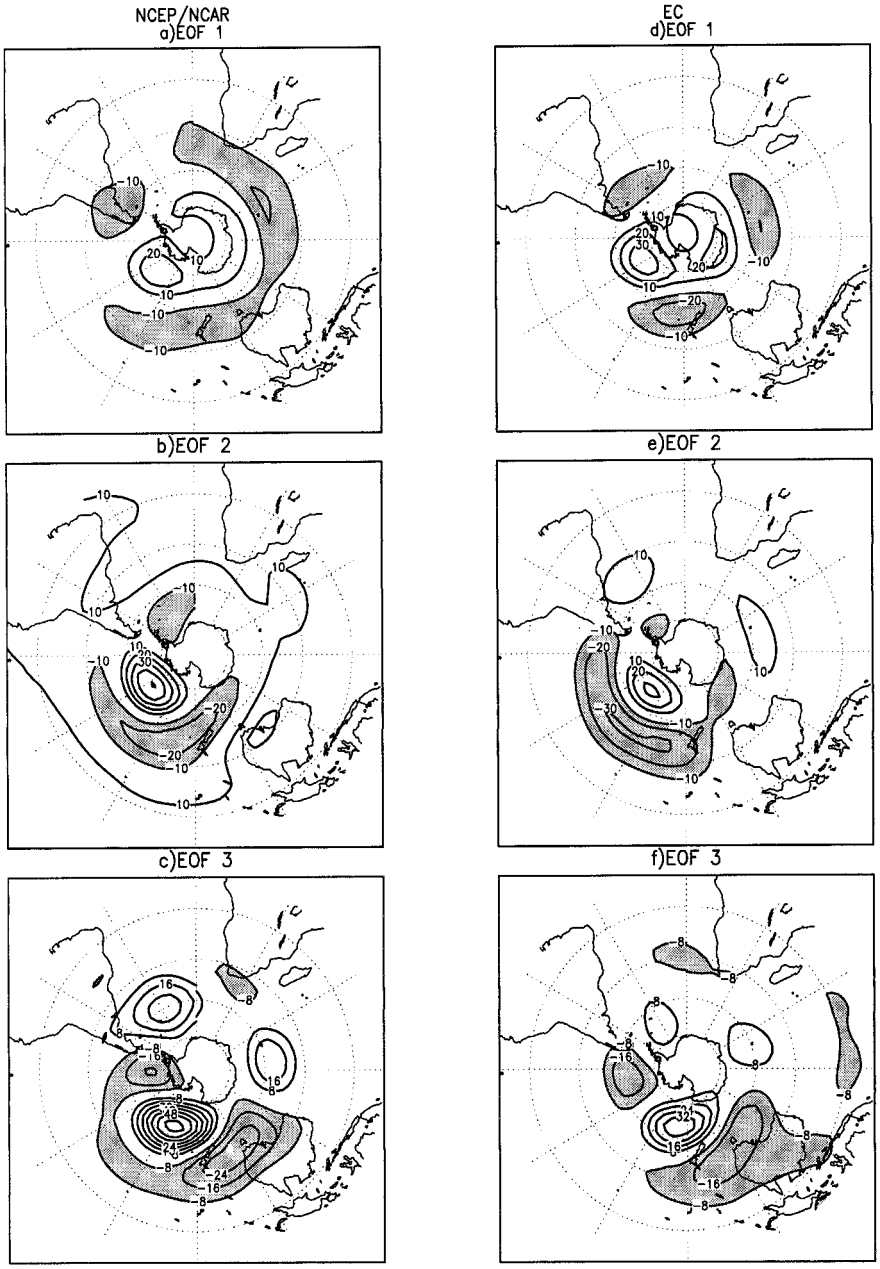

FIG. 1. (a) EOF1, (b) EOF2, and (c) −EOF3 for 500-hPa seasonal mean height anomalies from the NCEP–NCAR reanalysis. Contour interval is 10 nondimensional units for (a) and (b) and 8 nondimensional units for (c). Zero contours are omitted, negative values are shaded; (d) same as (a), but for the ECMWF reanalysis; (e) same as (d), but for EOF2; and (f) same as (d), but for −EOF3.

tion data. Both show a phase reversal between anomalies in the SH high and midlatitudes. It appears in both interdecadal band and the 50-day low-pass filtered data (Kidson 1999). This pattern was called the Antarctica Oscillation pattern by Thompson and Wallace (2000). This pattern is related to the zonal mean zonal wind indexes. It is associated with the zonal wind pattern with a maximum near 60°S and a minimum near 40°S (Kidson 1988a). The pattern is batrotropic (Kidson 1988a) and appears in both winter and summer.

EOF2 and EOF3 are degenerate, but both appear as rotated EOFs. They depict wave-3 patterns in quadrature with each other and a well-defined wave train from the tropical Pacific to Argentina with large amplitudes in the Pacific–South America sector. They are referred to as the PSA teleconnection patterns (Ghil and Mo 1991).

PSA1 (EOF2) associated with enhanced convection in the tropical central Pacific has been identified by Karoly (1989) as the major atmospheric response to ENSO in the SH. PSA1 also resembles REOF1 obtained by Karoly et al. (1996).

The monthly mean 500-hPa height anomalies were projected onto EOFs to obtain the PCs. They are referred to as the SH PCs and are plotted in Fig. 2 after taking a 24-month running average. In general, SH PC1 shows a downward trend that indicates heights decreasing over Antarctica and increasing at midlatitudes. The low-frequency band with fluctuations greater than 60 months explains 64% of the total variance. SH PC1 started to increase after 1963 and reached a maximum in 1966. After 1966, the general downward trend continued to the present with few exceptions. It briefly increased from 1970 to 1972, and from 1978 to 1981, and from 1990 to 1993. RPC2 of Karoly et al. (1996) shows a similar trend but their maximum occurred in 1972 while SH PC1 shows a weak maximum in 1972, and a stronger maximum in 1963. The differences may be caused by the uneven distribution of stations. EOF analysis on station data tends to emphasize features in the data rich areas. EOF1 is associated with the decrease of the sea level pressure over Antarctica. The correlation between SH PC1 and sea level pressure anomalies averaged from 70° to 90°S is 0.95. Van Loon et al. (1993) also observed the falling of sea level pressure over high latitudes and the rising of sea level pressure over areas near New Zealand and South America from 1972 to 1989 in the Australian analyses. Jones and Wigley (1988) compared the mean pressure from the Australian analysis from 1972 to 1985 and the reconstructed mean pressure from NOTOS data from 1957 to 1972. They also reported falling pressure over Antarctica.

Figure 2b shows SH PC2 (solid line) together with the negative Southern Oscillation index (SOI) defined as Tahiti minus Darwin sea level pressure anomaly (crosses). Overall, they track each other closely. This is consistent with findings of Karoly (1989) and Karoly et al. (1996) that PSA1 is the SH response to warm SSTA in the central Pacific and correlates well with the SOI. The sudden change of climate regimes (Trenberth 1990) around 1976 also occurred in SH PC2. One explanation is that there were more warm ENSO events after 1976. SH PC2 is related to ENSO. Therefore, SH PC2 was stronger after 1976. SH PC3 has more high-frequency components than SH PC1 and SH PC2. The high-frequency band explains about 78% of the total variance. It will be shown later that the dominant mode of SH PC3 is the quasi-biennial signal.

4. SSTA modes

Rotated EOF analysis was performed on seasonal mean SSTAs. All seasons were pooled together REOF1 (Fig. 3a) is also the first unrotated EOF and it explains about 27% of the total variance. It is referred as REOF1 (total). It is also the first EOF in the high-frequency band (less than 60 months) and it explains 28% of the total variance in that band. Figure 3a shows a typical ENSO pattern (Rasmusson and Carpenter 1982). It shows positive loadings extending from the eastern Pacific to the central Pacific with a maximum located at 100°W along the equator.

The REOF calculations were repeated for SSTAs in the low-frequency band (greater than 60 months). REOF1 low pass (LP) and REOF2 (LP) explain 33.4% and 8.4% of the variance in the low-frequency band, respectively. REOF1 (Fig. 3b) shows a pattern that resembles ENSO (Fig. 3a) with positive loading in the central-eastern Pacific, but the maximum is located in the central Pacific near 160°W. EOF2 (LP) (Fig. 3c) has positive loadings in all three southern oceans and negative loadings in the North Atlantic and the North Pacific.

5. Linkages between the SH circulation regimes and SSTAs

a. Association with SSTAs

In this section, seasonal mean SSTAs were regressed upon PCs (Fig. 2 solid lines). All seasons were pooled together. The SSTA pattern generated by regressing SSTAs upon SH PC1 (Fig. 4a) indicates that the downward trend of SH PC1 (Fig. 2a) is associated with warming over the eastern Pacific, the California coast, the South Atlantic and the Indian Ocean and cooling over the North Pacific and the North Atlantic. Most contributions are from the low-frequency band. It resembles SST REOF2 (LP) (Fig. 3c). The close association can be demonstrated by plotting SH PC1 together with −SST RPC2 (LP) in Fig. 5a. The SH PC1 was smoothed by applying a 5-yr running average before plotting. The correlation between them is 0.90. With 10 degrees of freedom, the correlation needs to be above 0.64 to be statistically significant at the 95% level.

The SSTA regression map associated with SH PC2 (Fig. 4b) shows a typical ENSO pattern (Rasmusson and Carpenter 1982). It resembles SST REOF1 (total) (Fig. 3a). Both maps show positive SSTA extending from the eastern Pacific to the central Pacific with negative SSTA over the North Pacific and the South Pacific and weak positive anomalies over the Indian Ocean. The SH response to that pattern is the PSA1 wave train as demonstrated by the high correlation (0.73) between SH PC2 (Fig. 5b, solid line) and SST RPC1 (total) (cross). The same pattern appears in the high-frequency band (not shown). The high-pass filtered SH PC2 and SST RPC1 (total) are given in Fig. 5c and the correlation between them is 0.75. In the low-frequency band, SH PC2 after taking a 5-yr running average (Fig. 5d, solid line) and the SST RPC1 (LP) (crosses) both show the abrupt change after 1976. The correlation between them is 0.81. In the low-frequency band, the regression map

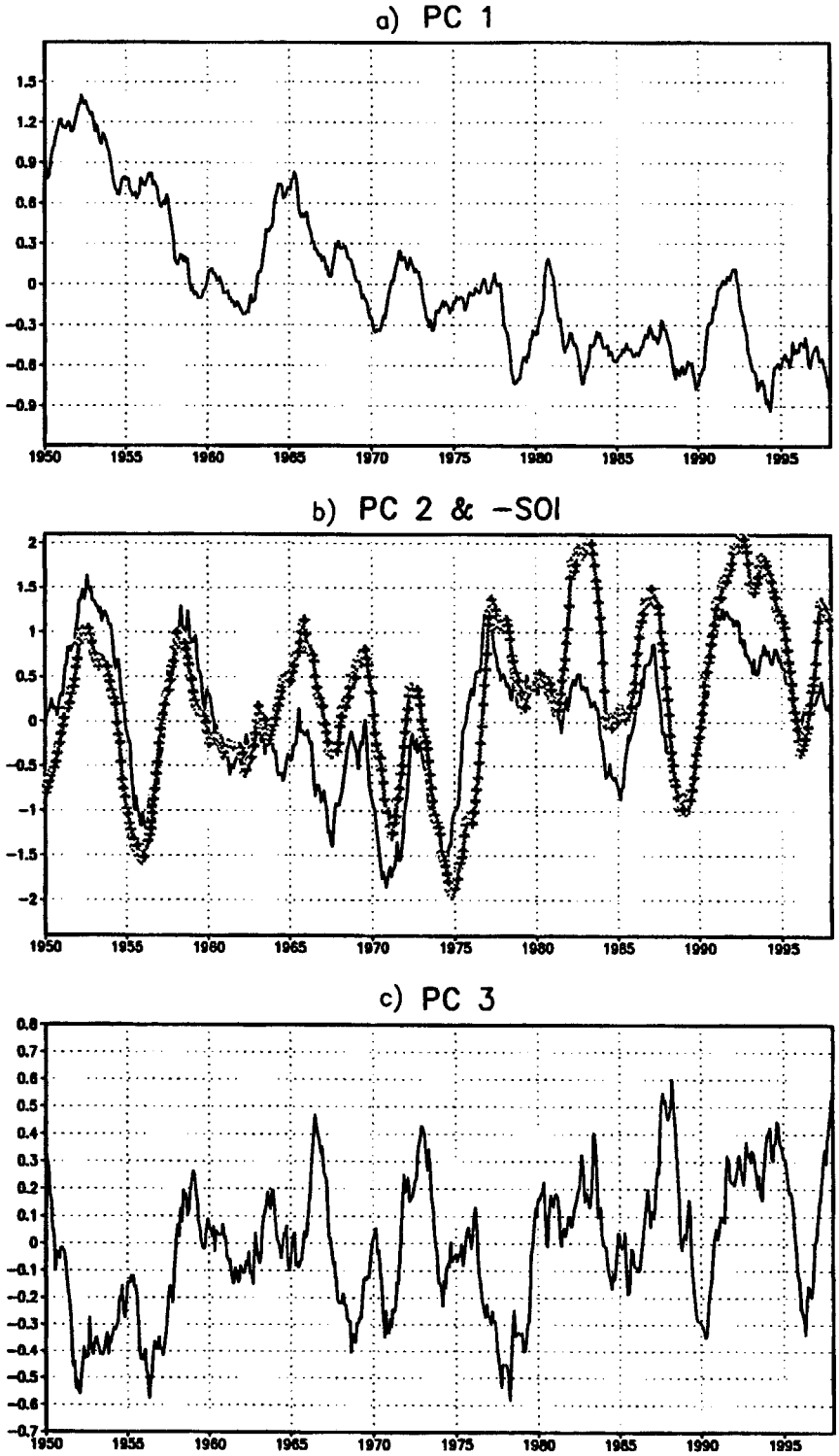

FIG. 2. The 24-month running means of normalized (a) PC1, (b) PC2 (solid line) and negative SOI (crosses), and (c) PC3.

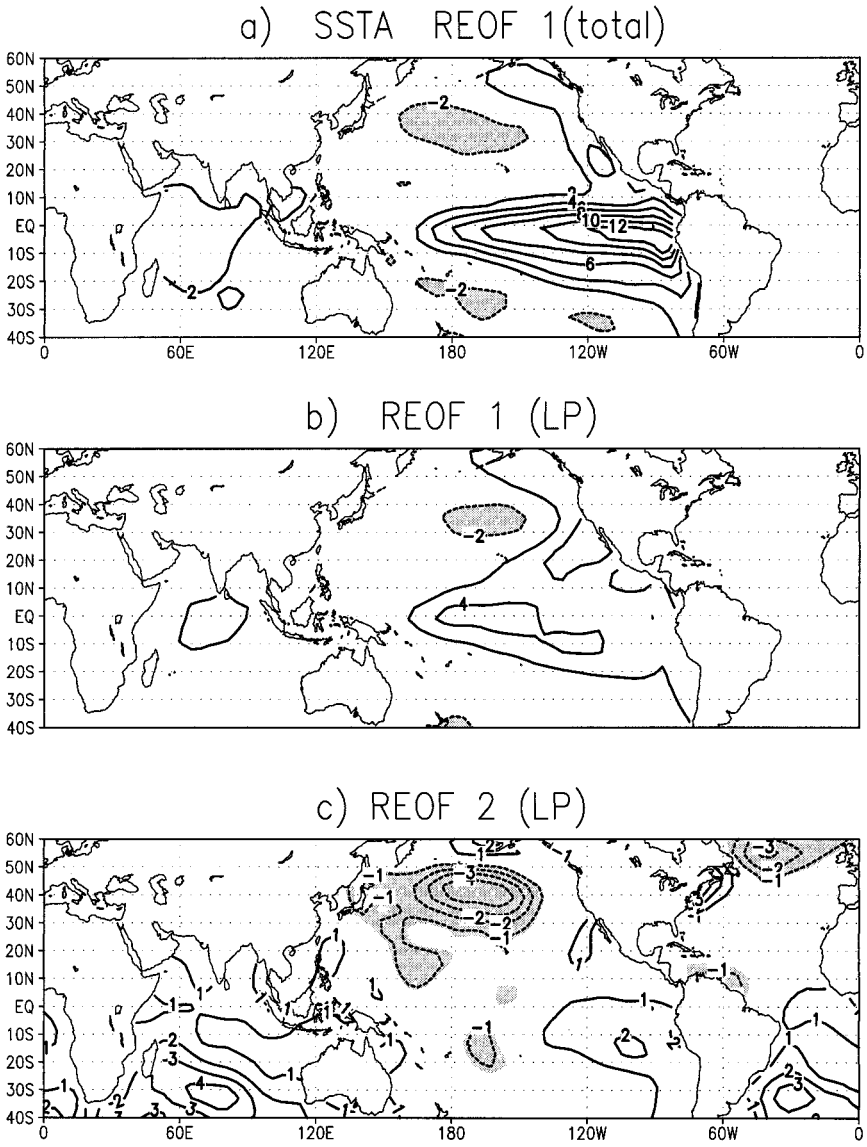

FIG. 3. (a) REOF1 (total) for seasonal mean SSTAs. Contour interval is 2 nondimensional units. Negative loadings are shaded, (b) same as (a), but for REOF1 (LP) for low-pass filtered SSTAs, and (c) same as (a), but for REOF2 (LP). Contour interval is 1 nondimensional unit.

of SSTA against SH PC2 resembles REOF1 (LP) (not shown) consistent with Fig. 5d. Regression analysis was repeated for seasonal means for December–February and June–August separately. They are similar but anomalies for December–February are slightly weaker.

The SSTA regression map against SH PC3 shows weak positive anomalies in the Indian Ocean (Fig. 4c). This map does not pass the field significant test. The reason is that the linkages between SH PC3 and SSTAs are seasonal dependent and strong correlations occur in spring.

Simultaneous correlations between SH PC3 and SSTA were obtained for each season separately. Anomalies were not filtered. Each season is considered as one degree of freedom. The values greater than 0.28 are statistically significant at the 95% level. Correlations were strong in September–November (Fig. 6c). It shows positive correlations in all three oceans south of 10°N with the strongest correlations located in the Indian Ocean and negative correlations extend southward from Australia to the South Pacific Convergence Zone. In contrast, the correlation map between seasonal mean SSTAs and SH PC2 (Fig. 6a) shows significant correlations in the Pacific. Figure 6c resembles the SSTA composite of the quasi-biennial mode for September–November (Rasmusson et al. 1990) and the quasi-biennial composite obtained by Barnett (1991) based on complex EOF analysis. Other studies have also found

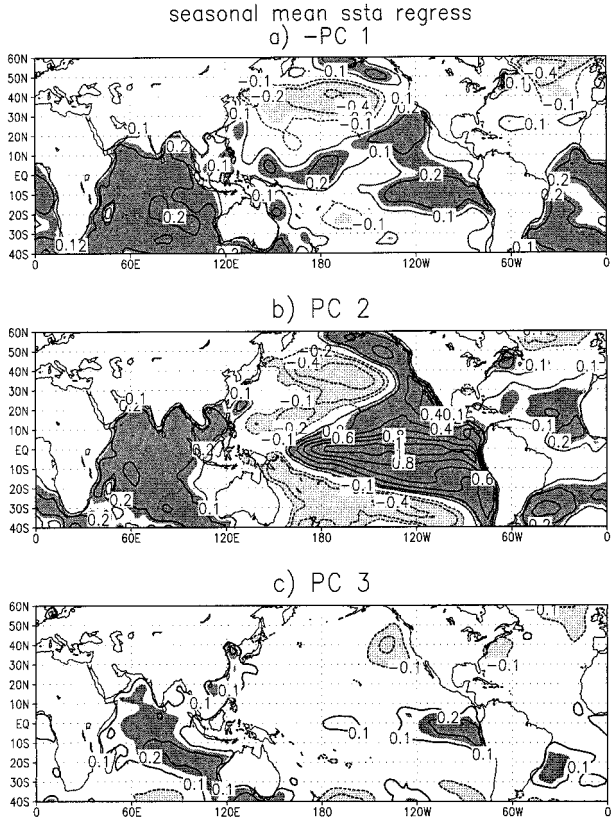

FIG. 4. Regression map of seasonal mean SSTAs against (a) normalized (−SH PC1), (b) SH PC2, and SH PC3 time series. Contour interval 0.2°C per standard deviation of SHPCs. Coutour −0.1 and 0.1 are added. Zero contours are omitted. Areas where positive (negative) values are statistically significant at the 95% level are shaded dark (light).

the quasi-biennial signal in the South Pacific near Australia and New Zealand (Trenberth 1975), and over the Indian Ocean (Allan et al. 1995). Their composites show that the quasi-biennial mode starts to develop during the Asian monsoon season in the Indian–Pacific sector. When the SSTAs in the Indian Ocean reach a maximum in September–November, the quasi-biennial mode reaches its maximum. That is the season in which correlations between SSTA and SH PC3 are the strongest (Fig. 6c). For all other seasons, correlations are only statistically significant in the Indian Ocean and maps do not pass the field significant test of Livezey and Chen (1983). The correlation map for June–August is given in Fig. 6b as an example. The significant correlations are located over the Indian Ocean, but correlations are weak in the Pacific.

b. Long-term trends and low-pass filtered anomalies

There are two SSTA modes in the low-frequency band (longer than 60 months) associated with long-term changes in the SH circulation. SST REOF1 (LP) (Figs. 3b and 5d) represents the abrupt warming of SSTA in the central and eastern Pacific after 1976 and it is associated with the intensification of PSA1. SST REOF2 (LP) (Fig. 3c) indicates gradual warming over three oceans in the SH (Fig. 5a) and it is associated with the downward trend of SH PC1. In the high-pass band, the dominant signal is ENSO and the response to ENSO in the SH is PSA1.

Garreaud and Battisti (1999) studied the interannual and interdecadal variability in the SH based on the cold tongue index (CT) defined as the average of SSTA over the equatorial Pacific (6°S–6°N, 190°–80°W). They found that the response in the SH to the 6-yr high-pass filtered CT (CT*) is PSA1. The CT* is the same as the high-pass filtered SST RPC1 (total). The correlation between them is 0.98. The response in the SH to CT* is high-pass filtered SH PC2 as indicated by Fig. 5f. The correlation between two time series is 0.96. Their CT* is the high-pass filtered SST RPC1 (total) here and the response in the SH is the PSA1 wave train.

They then fitted PC1 associated with the first EOF-mode of monthly mean SSTA to CT* and defined the residual (GR) as their interdecadal index. They took out the interannual signal of SSTA over the central-eastern Pacific so GR contains both the low-frequency changes in the central Pacific and changes in the southern oceans. The regression map of SSTA upon GR (their Fig. 5a) shows a mixture of REOF1 and REOF2 in the LP band (Figs. 3b and 3c).

To verify this, the standardized GR reproduced in Fig. 5e (solid line) is linear square fitted to the standardized RPC1 (LP) and RPC2 (LP) time series.

$$\mathrm{GR} \sim \mathrm{GR\ (fitted)} = 0.03 + 0.85\ \mathrm{RPC1} + 0.18\ \mathrm{RPC2}$$

Both GR and GR (fitted) are given in Fig. 5e. The correlation between them is 0.93. This indicates that GR contains both RPC1 (LP) and RPC2 (LP) signals. The ENSO-like SSTA pattern (Gareaud and Battisti 1999; Zhang et al. 1997) is a combination of the first two REOFs in the low-frequency band. Therefore, the associated circulation anomalies in the SH have a mixture of SH EOF1 and EOF2.

The association between convection in the Pacific and PSA1 is well known. Next, the circulation features associated with SH PC1 are discussed. The convection pattern is represented by the regression map of the 200-hPa divergence (Fig. 7a, shaded). The downward trend of SH PC1 is associated with enhanced convection (more divergence, dark shading) over the eastern Pacific and Central America in the area of warm SSTAs (Figs. 3c, 4a) and suppressed convection (less divergence, light shading) over the central Pacific, where SSTAs are weak. Positive anomalies (more divergence) are also located over the Indian Ocean. The 200-hPa streamfunction map shows a wavenumber-1 structure in the Tropics. Positive anomalies extend from South America through Africa to the Indian Ocean in the SH while negative anomalies extend from the central Pacific

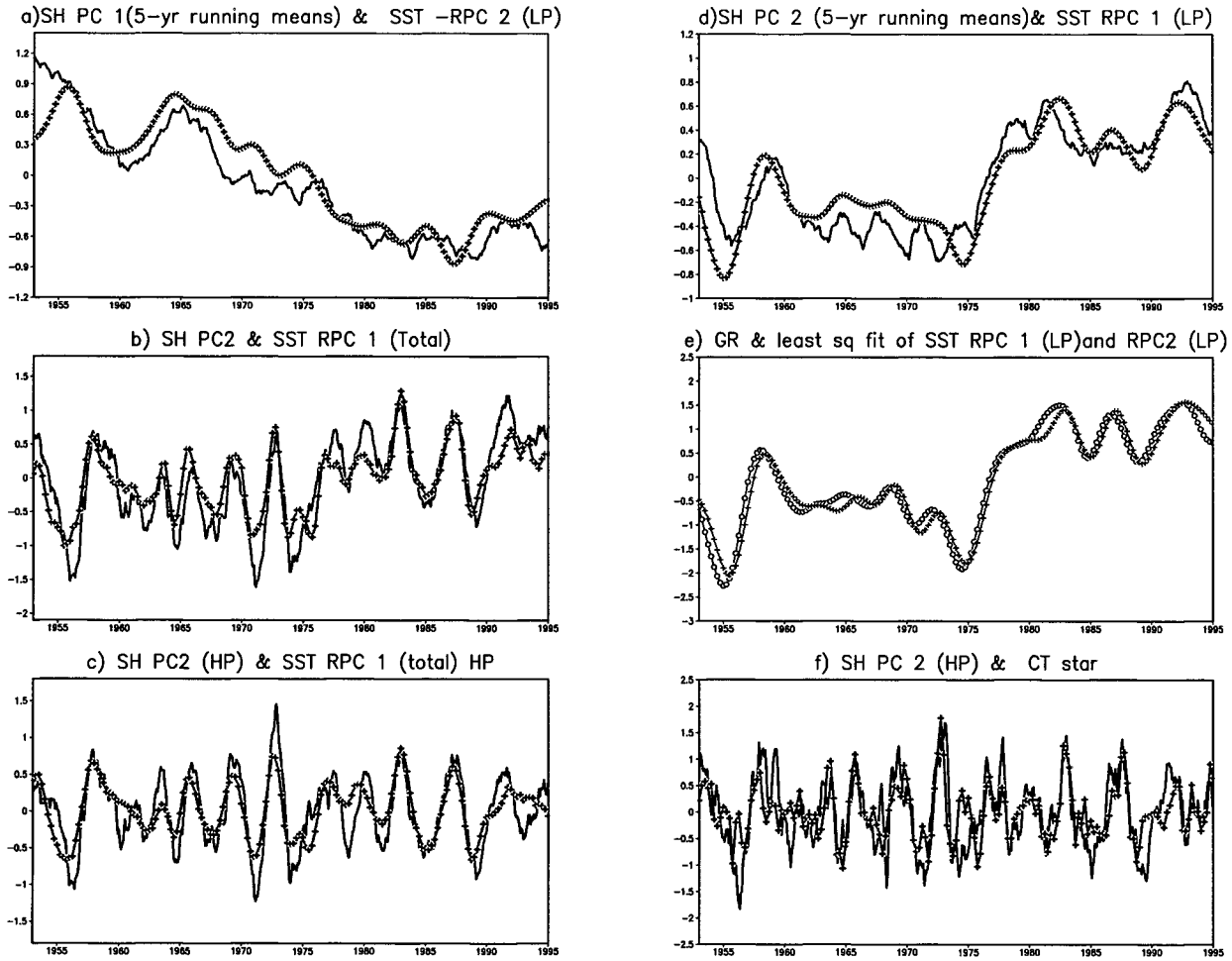

FIG. 5. (a) Normalized time series of SH PC1 (solid line) smoothed by applying 5-yr running average and −RPC2 (LP) × 0.5 (crosses) for low-pass filtered SSTAs; (b) normalized time series of SH PC2 (solid line) and RPC1 × 0.5 (total) (crosses) for seasonal mean SSTAs; (c) same as (b), but for high-pass filtered time series; (d) normalized time series of SH PC2 (solid line) smoothed by applying 5-yr running average and RPC1 (LP) × 0.5 (crosses); (e) GR time series (solid line) of Garreaud and Battisti (1999) and the least squares fit of GR (crossed) to RPC1 (LP) and RPC2 (LP); and (f) normalized high-pass filtered SH PC2 (solid line) and CT* × 0.5 of Garreaud and Battisti.

southeastward to Argentina. Anomalies north and south of the equator are opposite in phase.

In the SH, the 200-hPa streamfunction anomalies are consistent with EOF1. The streamfunction pattern implies the weakening of the subtropical jet over Australia and strengthening of the jet at high latitudes. This is consistent with the 200-hPa zonal mean *u*-wind anomalies regressed upon SH PC1 (Fig. 7b). There are more zonal mean westerly anomalies over high latitudes (50°–60°S) and less westerly anomalies over the subtropics (30°–40°S). Similar connection between positive zonal wind index and negative EOF1 has been found by Kidson (1988b) using the monthly mean data from the Australian analyses. Consistent with findings of Thompson and Wallace (2000), the fall of heights over Antarctica is associated with a contracted polar vortex. In the extratropics, height anomalies associated with SH EOF1 are barotropic. Positive anomalies in midlatitudes are consistent with weaker winds. Weaker winds are consistent with warmer temperatures in the southern oceans.

c. Variations in the high-frequency band (48-month mode and quasi-biennial mode)

Rasmusson et al. (1990) used SSA to separate ENSO variability into the low-frequency component in the 40–48-month band (his low-frequency component) and the quasi-biennial component in the 22–30-month band. Both modes are considered as fundamental elements of ENSO variability. Strong ENSO events tend to occur when the two components are in phase with each other. These two modes also were described by Allan et al (1995) in their study on the decadal changes in the Indian Ocean. In this section, these two modes of SSTAs and the corresponding anomalies in the SH are discussed.

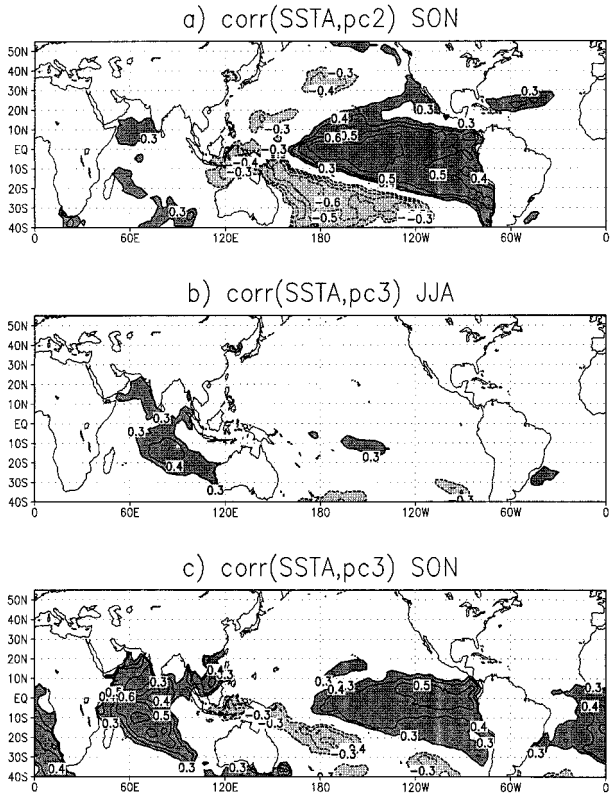

FIG. 6. (a) Correlation map between seasonal mean SSTA and SH PC2 for Sep–Nov. Contour interval 0.1. Areas where positive (negative) correlations are statistically significant at the 95% level are shaded dark (light), and (b) same as (a), but the correlation map between SSTA and PC3 for Jun–Aug and (c) same as (b), but for Sep–Nov.

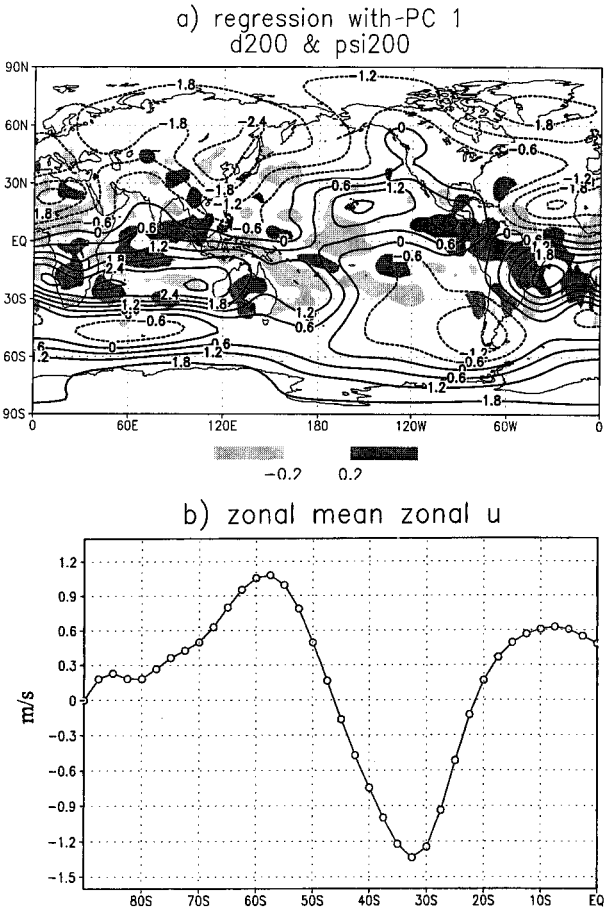

FIG. 7. Same as Fig. 4a, but for 200-hPa divergence (shaded) and 200-hPa streamfunction anomalies. The unit for divergence is $0.2 \times 10^{-6}\ s^{-1}$. Contour interval for streamfunction anomalies is $0.6 \times 10^{+06}\ m\ s^{-2}$. Negative contours are dashed, and (b) same as (a), but for the zonal mean zonal wind anomalies.

The power spectra of monthly mean PCs were obtained by using the Blakman–Turkey correlation method. There is a total of 600 points in the time series. If one season is considered as one degree of freedom, then the band width is estimated as 0.0086 (Jenkin and Watts 1968). There is no statistically significant peaks in SH PC1 consistent with findings of Kidson (1988a,b). The SH PC2 has only one peak at 48 months (Fig. 8a). The quasi-biennial mode of 24–26 months is the dominant mode in SH PC3. The second weak peak is near 36–40 months (Fig. 4b). These results are reproduced using SSA. SSA is unique because it allows the reconstruction of each mode. Therefore, it gives information on the variations of each mode separately.

SSA was performed on SH PC2 and SH PC3 (Figs. 2b and 2c) associated with PSAs and SST RPC1 (total). The window size used was 61. Before performing SSA, all time series were high-pass filtered to concentrated in the interannual band with fluctuations less than 60 months.

For the SSTA RPC1 time series, the first two SSA modes have two T-EOFs (EOF in the time domain) in quadrature with each other with degenerated eigenvalues. They represent an oscillation with a period of 40–48 months and they explain 42% of the total variance. This mode is referred to as the 48-month mode. The next two T-EOFs represent an oscillation with a period of 24–26 months. It is in the range of the quasi-biennial oscillation and it explains about 24% of the total variance. Results agree with Rasmusson et al. (1990) that ENSO variability has both the 48-month mode and the quasi-biennial mode.

For SH PC2 (PSA1), SSA results show that the first two T-EOFs represent an oscillation with a period of 48 months. This mode explains about 14% of the total variance. There is no quasi-biennial mode in the SH PC2 time series consistent with power spectral density obtained using the Blakman–Turkey window (Fig. 8a). As expected, the first SSA mode for PC3 (PSA2) is the quasi-biennial mode with a period of 26 months. It explains about 8% of the total variance.

Both SST RPC1 (total) and PSA PCs have the 48-month mode and the quasi-biennial mode. For both variables, the original time series can be projected onto T-EOFs to get the corresponding T-PCs. Time series

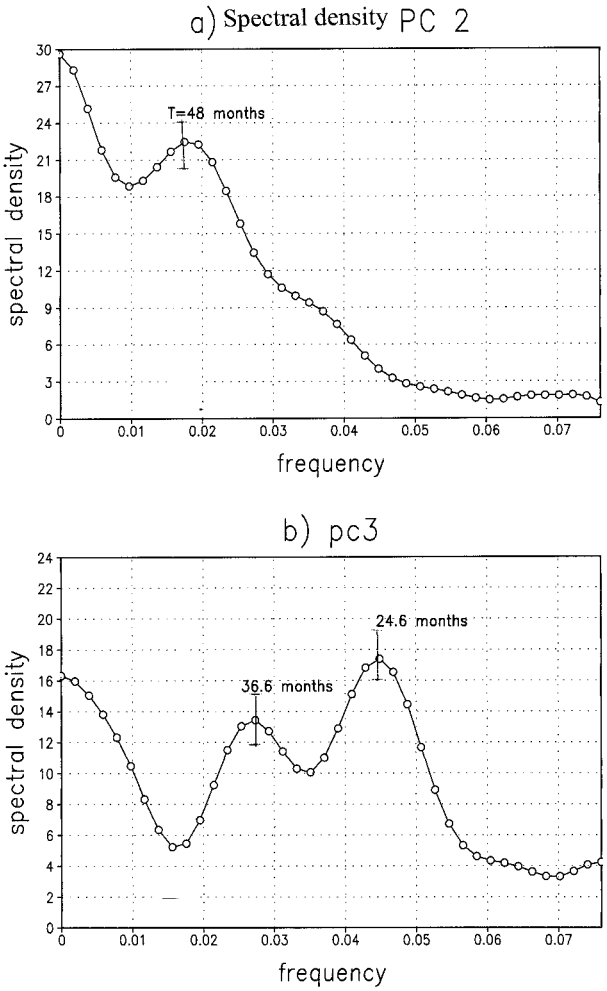

FIG. 8. Spectral density of SH PC2 and SH PC3. The 95% confidence levels are given.

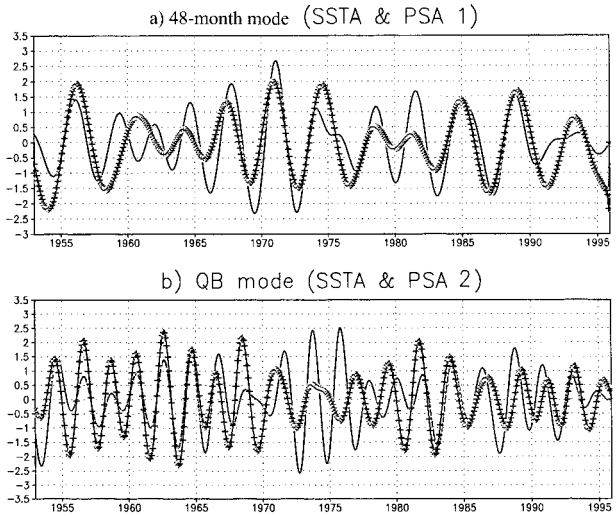

FIG. 9. (a) Normalized reconstructed time series for the PSA1 (crosses) and SSTA (dark line) 48-month mode; (b) same as (a), but for the PSA2 and SSTA quasi-biennial components.

corresponding to the 48-month mode (the quasi-biennial component) can be reconstructed by adding up the associated pair of T-EOFs and the T-PCs for each mode. Figure 9 shows the reconstructed time series for SSTA 48-month mode (dark line) and PSA 48-month mode (crosses). Except for the period from 1960 to 1964, there is a very good correspondence between two curves. From 1960 to 1964, the SSTA 48-month mode was weak and the oscillation was less regular so the response was also weak. The SSTA and PSA reconstructed time series for the quasi-biennial mode tracked each other well from 1950 to 1970. In the 1970s, the PSA quasi-biennial mode was weak and irregular. After 1981, two curves again followed each other closely. This suggests that PSA1 responds to the 48-month mode of ENSO, while PSA2 is associated with the quasi-biennial component of ENSO.

To examine the convection pattern associated with the 48-month mode and quasi-biennial mode, the 200-hPa streamfunction anomalies and anomalous divergence were regressed upon the reconstructed PSA 48-month mode and quasi-biennial time series (Figs. 9a and 9b crosses). The 48-month mode (Fig. 10a) shows the typical ENSO convection pattern with enhanced convection in the central and eastern Pacific at locations of warm SSTAs (Fig. 6a) and suppressed convection in the subtropics and the western Pacific. The response of the 200-hPa streamfunction anomalies shows a dipole straddling the equator and a PSA2 wave train in the SH.

The convection pattern revealed by the regression map of the 200-hPa divergence for the quasi-biennial mode (Fig. 10b) is very different from the 48-month mode. It shows a three-cell pattern in the Tropics. Enhanced convection (more divergence, dark shading) is located over the central Pacific, but it does not extend to the eastern Pacific. It also shows enhanced convection over the Indian Ocean and suppressed convection in the western Pacific. In the Tropics, enhanced convection occurs at the location of warm SSTAs (Fig. 6c). The 200-hPa streamfunction also shows a dipole in the Tropics, but it is located west of the dipole associated with the 48-month mode. In the SH, there is a PSA2 wave train as expected. For both components, responses in the Northern Hemisphere are weak.

6. Conclusions

The long-term trends and interannual variations of circulation regimes in the SH were examined using the NCEP–NCAR reanalysis from 1949 to the present. Results were compared with the changes observed in the station observations (Karoly et al. 1996) and the Australian analyses (van Loon et al. 1993).

On the decadal timescales with fluctuations longer than 60 months, the leading mode in the SH (SH EOF1) shows a zonal symmetric pattern with a phase reversal

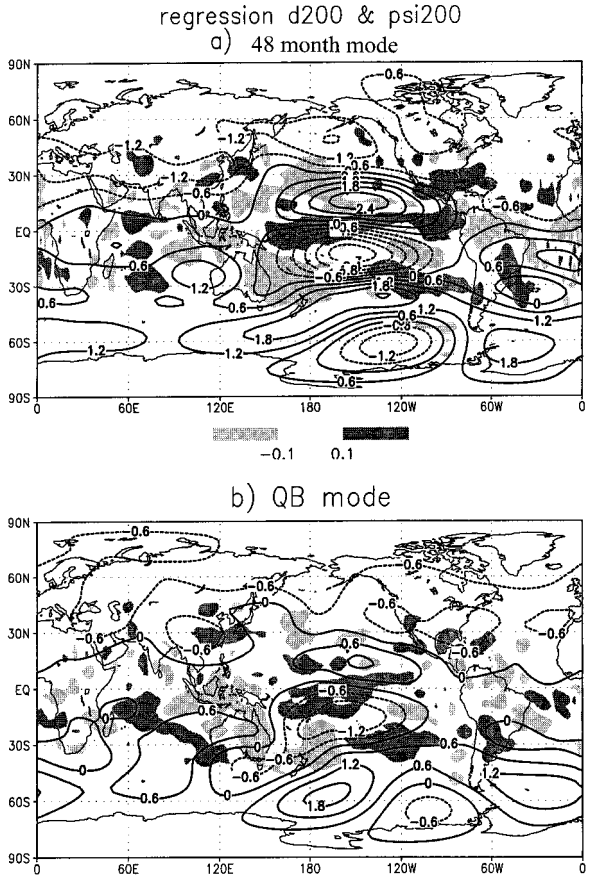

FIG. 10. Spatial patterns generated by regressing 200-hPa divergence (shaded) and streamfunction anomalies upon the normalized reconstructed time series for the PSA 48-month mode and the PSA quasi-biennial component (Fig. 9). The unit for divergence is 0.2×10^{-6} s^{-1}. Contour interval is $0.6 \times 10^{+06}$ m s^{-2} for the streamfunction anomalies. Negative contours are dashed.

between high and midlatitudes. This mode appears as the second mode from station data analysis (Karoly et al. 1996). The downward trend of height over Antarctica has been observed in the Australian analyses from 1972 to 1989 by van Loon et al. (1993) and station observations (Hurrell and van Loon 1994). This mode is associated with the second REOF mode in low-pass filtered SSTAs with gradual warming in the eastern Pacific and the South Atlantic and the Indian Ocean and cooling in the North Pacific and the North Atlantic.

EOF1 resembles the zonally symmetric pattern obtained by Thompson and Wallace (2000) which they called the Antarctica Oscillation (AAO) using monthly mean data. They also found similarity between the AAO and the Arctic Oscillation (AO) in the Northern Hemisphere. However, the regression map (Fig. 7a) of 200-hPa streamfuncion upon the low-pass filtered SH PC1 does not show the AO pattern in the Northern Hemisphere. It could be due to seasonality, but it is also possible that the AO and the AAO have different origins. More research is needed in this area.

In addition to REOF2 (LP) mode, the long-term changes in the SH is also related to REOF1 (LP), which shows the abrupt warming after 1976 in the central and eastern Pacific. The associated change in the SH is PSA1. Zhang et al. (1997) and Garreaud and Battisti (1999) show that the leading mode of SSTAs in the low-frequency band is an ENSO-like mode. Their mode shows strong positive loadings in the central and eastern Pacific with the maximum located at 160°W and slightly weaker positive loadings in the three southern oceans. In the Northern Hemisphere, cooler SSTAs are located in the North Pacific and the North Atlantic. This mode is a combination of REOF1 (LP) and REOF2 (LP) here, therefore, the associated circulation anomalies in the SH resemble the mixture of SH EOF1 and PSA1.

Both PSAs are associated with ENSO variability. PSA2 has bean linked to warm ENSO events (Karoly 1989), and SOI (Karoly et al. 1996). SSA analysis indicates that PSA1 is the response to the 48-month mode of the ENSO signal. The SSTA pattern shows warming in the central-eastern Pacific. PSA2 responds to the quasi-biennial component of the ENSO signal. It is associated with warm SSTA in the central Pacific and the Indian Ocean and cooling in the western Pacific.

REFERENCES

Allan, R. J., J. A. Lindesay, and C. J. Reason, 1995: Multidecadal variability in the climate system over the Indian Ocean region during the Austral summer. *J. Climate,* **8,** 1853–1873.

Barnett, T. P., 1991: The interaction of multiple time scales in the tropical climate system. *J. Climate,* **4,** 269–285.

Garreaud, R., and D. S. Battisti, 1999: Interannual and interdecadal (ENSO-like) variability in the Southern Hemisphere tropospheric circulation. *J. Climate,* **12,** 2113–2123.

Ghil, M., and K. C. Mo, 1991: Intraseasonal oscillations in the global atmosphere. Part II: Southern Hemisphere. *J. Atmos. Sci.,* **48,** 480–490.

Hurrell, J. W., and H. van Loon, 1994: A modulation of the atmospheric annual cycle in the Southern Hemisphere. *Tellus,* **46A,** 325–338.

Jenkin, G. M., and D. G. Watts, 1968: *Spectral Analysis and Its Applications.* Holden-Day, 525 pp.

Jones, P. D., and T. M. L. Wigley, 1988: Antarctica gridded sea level pressure data: An analysis and reconstruction back to 1957. *J. Climate,* **1,** 1199–1220.

——, and R. J. Allan, 1998: Climate change and long term climate variability. *Meteorology of the Southern Hemisphere,* D. J. Karoly and D. G. Vincent, Eds., Amer. Meteor. Soc., 337–363.

Kalnay, E., and Coauthors, 1996: The NCEP/NCAR 40-Year Reanalysis Project. *Bull. Amer. Meteor. Soc.,* **77,** 437–471.

Karoly, D. J., 1989: Southern Hemisphere circulation features associated with El Niño–Southern Oscillation events. *J. Climate,* **2,** 1239–1251.

——, P. Hope, and P. D. Jones, 1996: Decadal variations for the Southern Hemisphere circulation. *J. Climatol.,* **16,** 723–738.

Kidson, J. W., 1988a: Interannual variations in the Southern Hemisphere circulation. *J. Climate,* **1,** 1177–1198.

——, 1988b: Indices of the Southern Hemisphere zonal wind. *J. Climate,* **1,** 183–194.

——, 1999: Principal modes of Southern Hemisphere low-frequency variability obtained from NCEP–NCAR reanalyses. *J. Climate,* **12,** 2808–2830.

Kiladis, G. N., and K. C. Mo, 1998: Interannual and intraseasonal

variability in the Southern Hemisphere. *Meteorology of the Southern Hemisphere,* D. J. Karoly and D. G. Vincent, Eds., Amer. Meteor. Soc., 307–336.

Lau, K.-M., P. J. Sheu, and I.-S. Kang, 1994: Multiscale low-frequency circulation modes in the global atmosphere. *J. Atmos. Sci.,* **51,** 1169–1193.

Livezey, R. E., and W. Y. Chen, 1983: Statistical field significance and determination by Monte Carlo techniques. *Mon. Wea. Rev.,* **111,** 46–59.

O'Lenic, E. A., and R. E. Livezey, 1988: Practical considerations in the use of rotated principal component analysis (RPCA) in diagnostic studies of upper air height fields. *Mon. Wea. Rev.,* **116,** 1682–1689.

Papoulis, A., 1973: Minimum bias windows for high resolution spectral estimates. *IEEE Trans. Inf. Theory,* **19,** 9–12.

Rasmusson, E. M., and T. H. Carpenter, 1982: Variations in tropical sea surface temperature and surface wind fields associated with the Southern Oscillation/El Niño. *Mon. Wea. Rev.,* **110,** 354–384.

——, X. Wang, and C. F. Ropelewski, 1990: The biennial component of ENSO variability. *J. Mar. Syst.,* **1,** 71–96.

Reason, C. J., R. J. Allan, and J. A. Lindesay, 1996: Dynamical response of the oceanic circulation and temperature in interdecadal variability in the surface winds over the Indian Ocean region. *J. Climate,* **9,** 97–114.

Rogers, J. C., and H. van Loon, 1982: Spatial variability of sea level pressure and 500 mb height anomalies over the Southern Hemisphere. *Mon. Wea. Rev.,* **110,** 1375–1392.

Smith, T. M., R. W. Reynolds, R. E. Livezey, and D. C. Stokes, 1996: Reconstruction of historical sea surface temperatures using empirical orthogonal functions. *J. Climate,* **9,** 1403–1420.

Thompson, D., and J. M. Wallace, 2000: Annular modes in the extratropical circulation. Part I: Month-to-month variability. *J. Climate,* **13,** 1000–1016.

Trenberth, K. E., 1975: A quasi-biennial standing wave in the Southern Hemisphere and interrelations with sea surface temperature. *Quart. J. Roy. Meteor. Soc.,* **101,** 55–74.

——, 1990: Recent observed interdecadal climate changes in the Northern Hemisphere. *Bull. Amer. Meteor. Soc.,* **71,** 988–993.

——, and J. W. Hurrell, 1994: Decadal atmospheric ocean variations in the Pacific. *Climate Dyn.,* **9,** 303–319.

Van Loon, H., J. W. Kidson, and A. N. Mullan, 1993: Decadal variation of the annual cycle in the Australian dataset. *J. Climate,* **6,** 1227–1231.

Vautard, R., and M. Ghil, 1989: Singular spectrum analysis in nonlinear dynamics with applications to paleoclimatic time series. *Physica D,* **35,** 392–424.

——, P. Yiou, and M. Ghil, 1992: Singular spectrum analysis: A toolkit for short, noisy chaotic signals. *Physica D,* **58,** 95–126.

Zhang, Y., J. M. Wallace, and D. S. Battisti, 1997: ENSO-like interdecadal variability: 1900–93. *J. Climate,* **10,** 1004–1020.